Mode of extension and rifting history of upper Tiburón and upper Delfín basins, northern Gulf of California

A. González-Fernández,[1] J. J. Dañobeitia,[2] L. A. Delgado-Argote,[1] F. Michaud,[3] D. Córdoba,[4] and R. Bartolomé[2]

Received 15 December 2003; revised 15 July 2004; accepted 20 September 2004; published 26 January 2005.

[1] The crustal structure of the northern Gulf of California transtensional margin has been investigated by a 280-km-long NW-SE profile, including deep multichannel seismic reflection and densely sampled refraction/wide-angle reflection seismic information combined with gravity modeling. The seismic and gravity modeling constrains two thinned crustal areas, corresponding to the upper Delfín and the upper Tiburón basins. On both sides of the profile, toward the Baja California Peninsula and the Mexico mainland, a progressive thickening of the continental crust is observed. Our results indicate that the crustal thickness is 19 km below the coastline, and it decreases to 14 and 17 km below the upper Delfín and upper Tiburón basins, respectively. In the area between both basins, the crust thickens to 19.5 km. There are significant lateral thickness variations for the different levels of the crust. The interpreted structure is consistent with the existence of an aborted rift below the upper Tiburón basin. Prominent dipping reflections in the multichannel data under upper Tiburón basin and the ridge between upper Tiburón and upper Delfín basins can be explained as a mylonite like zone related to a detachment fault. This interpretation suggests that the structural evolution of upper Tiburón basin could be controlled by a major fault that cuts through the upper crust and merges into a zone of subhorizontal reflections in the lower crust. The mode and locus of extension have evolved from a core complex in upper Tiburón to a narrow rift mode in upper Delfín basin.

Citation: González-Fernández, A., J. J. Dañobeitia, L. A. Delgado-Argote, F. Michaud, D. Córdoba, and R. Bartolomé (2005), Mode of extension and rifting history of upper Tiburón and upper Delfín basins, northern Gulf of California, *J. Geophys. Res.*, *110*, B01313, doi:10.1029/2003JB002941.

1. Introduction

[2] The transtensional rift system of the northern Gulf of California is the continuation to the south of the San Andreas fault system, and both constitute the present boundary between the Pacific and the North America plates. Until now, the deep structure of the Gulf of California has been mainly inferred from bathymetry, gravity and some low-resolution seismic refraction data. Some key information, like crustal thickness or the oceanic/continental nature of the crust, is poorly known at the present. *Phillips* [1964] obtained some deep crustal information using explosives as seismic sources and sonobuoys as recording instruments. His results sample scattered locations in the gulf, obtaining one-dimensional (1-D) seismic models and, in some cases, 2-D models based on flat discontinuities. However, no bathymetric data were used in these models, so the results have a certain degree of uncertainty. In most cases, the seismic energy did not reach the Moho discontinuity.

[3] The nearest area more intensely studied is the Imperial Valley region, where a transitional (not continental nor typical oceanic) type of crust, produced by rifting, intrusion and high sedimentation, with metamorphosed sedimentary rocks has been proposed [*Fuis et al.*, 1984], based on the interpretation of wide-angle seismic profiles and gravity modeling. A similar type of crust, with intrusive bodies interbedded with sediments, has been proposed for the Guaymas basin [*Einsele*, 1982; *Saunders et al.*, 1982; *Lonsdale*, 1985] and offshore Santa Rosalía [*Fabriol et al.*, 1999] (Figure 1). Other areas of the Gulf of California extensional province have been scarcely surveyed.

[4] Some gravity modeling, based on the limited refraction interpretations of *Phillips* [1964], has also been done [*Couch et al.*, 1991]. However, the nonuniqueness of this methodology, involving the interdependence of structure and density, implies a considerable degree of uncertainty.

[5] Most of the tectonic knowledge has been obtained from the geomorphologic interpretation of the bathymetric features [e.g., *Lonsdale*, 1989] and only locally from the combination of geophysical and bathymetric data [*Fabriol*

[1]Departamento de Geología, División de Ciencias de la Tierra, Centro de Investigación Cientifica y Educación Superior de Ensenada, Ensenada, Baja California, Mexico.
[2]Unidad de Tecnología Marina, Consejo Superior Investigación Cientificas, Barcelona, Spain.
[3]Observatoire Océanologique de Villefranche, Villefranche sur Mer, France.
[4]Departamento de Geofísica, Facultad de Ciencias Físicas, Universidad Complutense de Madrid, Madrid, Spain.

0148-0227/05/2003JB002941$09.00

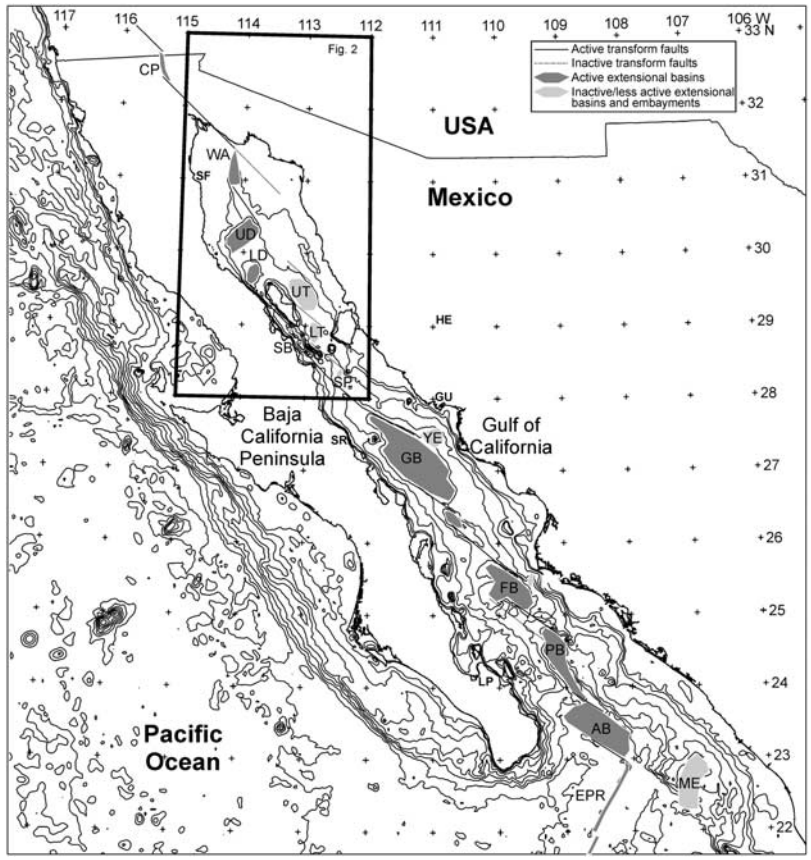

Figure 1. Location map. The rectangle shows the location of the study area. The dark and light gray shading areas correspond to the known active and inactive (or less active) extensional basins in the Gulf of California [after *Lonsdale*, 1989; *Fenby and Gastil*, 1991]. The main transform fault zones are also shown. Contour interval is 500 m [from *Smith and Sandwell*, 1997]. Additional contours are at 100 and 200 m. Basins are CP, Cerro Prieto; WA, Wagner; UD, upper Delfin; LD, lower Delfin; UT, upper Tiburón; LT, lower Tiburón; SB, Salsipuedes; SP, San Pedro Mártir; GB, Guaymas; FB, Farallón; PB, Pescadero; AB, Alarcón. Embayments are YE, Yaqui; ME, Mazatlán. Other features are EPR, East Pacific Rise; SF, San Felipe; HE, Hermosillo; GU, Guaymas; SR, Santa Rosalía; LP, La Paz.

et al., 1999]. In the central and southern Gulf of California this approach has proven quite successful. However, in the north, the high amount of sediments from the Colorado River has made it difficult to perform this type of interpretation. Furthermore, most of the bathymetric data available has been recorded with single beam echo sounders, most of them obtained before 1984 [*Ness and Lyle*, 1991], with limitations in navigation.

[6] The Guaymas basin (Figure 1) has been intensely surveyed [*Curray et al.*, 1982; *Lonsdale*, 1985]. The available data suggest a transitional type of crust, different from normal oceanic or continental crust [*Einsele*, 1982]. Here, in the upper crust, the high rate of sedimentation and probably the low rate of emplacement of magma do not promote significant eruptive activity, implying the formation of a thick layer of intercalated sills, altered sediments and some massive intrusions. The lower crust may be similar to typical oceanic crust [*Lonsdale*, 1985]. Development of transitional type of crust has been also documented offshore Santa Rosalía in the peninsular margin of the gulf [*Fabriol et al.*, 1999].

[7] From observation of magnetic anomaly lineations [*Larson et al.*, 1972; *Klitgord et al.*, 1974; *DeMets*, 1995], only the southernmost Gulf of California basin, the Alarcón basin, is composed of typical oceanic crust. Other gulf basins show no obvious pattern of magnetic lineations of the type that would be produced by seafloor spreading. The usual belief is that the basins to the north of the Alarcón basin have compositions similar to the Guaymas basin [*Larson et al.*, 1972], where the high sedimentation rates inhibit the extrusion of highly magnetized basalt, which are replaced by a process of sill and dike intrusion instead [*Vogt et al.*, 1970; *Irving*, 1970; *Einsele*, 1982]. However, in the northern Gulf of California, there is not enough evidence to know the nature of the crust or its structure. The understanding of the crustal type can provide an insight in the history of the opening of the Gulf of California.

[8] In the northern Gulf of California, the most detailed reflection seismic images, although only for the uppermost crust, were provided by *Henyey and Bischoff* [1973] and more recently by *González-Fernández et al.* [1999] and *Persaud et al.* [2003]. *Henyey and Bischoff* [1973] used a small (10 cubic inches, 0.16 L) air gun and a one-channel recorder, with a typical penetration of 0.2 s (all times quoted in seconds refer to two-way travel times (TWTT)). They proposed that the upper Delfín basin is a relatively

new spreading center, with spreading having occurred elsewhere in the northern Gulf of California at an earlier stage in its development. Earlier spreading may have taken place at a spreading center located along a transform fault east of Angel de la Guarda Island. Reviewing the *Phillips* [1964] data, *Henyey and Bischoff* [1973] also suggested that a high sedimentation rate can produce a basalt-sediment mixture due to injection of magma into sediments. As a result, the refraction data can be interpreted in terms of a continuous velocity-depth function rather than discrete layers, particularly near the spreading centers, in a similar fashion to the proposed structure for the Imperial Valley region discussed by *Fuis et al.* [1984]. The fault map/structural patterns presented in their work (a reinterpretation is given by *Fenby and Gastil* [1991]) support a diffuse distribution of strain in a big area rather than localized in the neighborhood of spreading centers.

[9] *González-Fernández et al.* [1999] and *Persaud et al.* [2003] used a stronger seismic source (150 cubic inches, 2.5 L) and a multichannel (48 channel) streamer, providing high-resolution images of the first 2–3 s, namely, the first sedimentary layers, down to the basement in some areas. These seismic images show again a diffuse distribution of strain, with clear intense normal faulting that frequently displaces recent sediments, although buried faults were also observed. The only magmatic activity found was located in the upper Delfín basin, where there are outcrops on the seafloor [*Persaud et al.*, 2003]. The strong sedimentation and shallow penetration did not allow imaging of magmatic products in other areas, except for some isolated submarine volcanoes. Lava bodies were interpreted from backscattering images, magnetic and seismic data for the upper Delfín basin and mainly along the Ballenas-Salsipuedes channel [*Frías-Camacho et al.*, 1999; *Delgado-Argote*, 2000; *Paz-López et al.*, 2000; *Paz-López*, 2000] using CORTES-P96 cruise data [*Dañobeitia et al.*, 1997].

[10] The data presented here correspond to geophysical line P313, acquired using the R/V *Hespérides* during cruise CORTES-P96 in 1996 [*Dañobeitia et al.*, 1997]. We report here the main findings of our deep seismic and gravity study and discuss their implications.

2. Tectonic Setting

[11] The study area comprises the upper Delfín and upper Tiburón basins (Figures 1 and 2). The known stratigraphy of the northern Gulf of California can be briefly summarized as a sequence of Pliocene to recent marine sediments of sand and limolites [*Pérez-Cruz*, 1980]. The age of the youngest sediments are inferred by a Mexican petroleum company PEMEX borehole (Seri-1, PEMEX unpublished, see Figure 2), based on estimated sedimentation rates. PEMEX data [*Pérez-Cruz*, 1980] and sediment samples collected by *Van Andel* [1964] indicate recent high sedimentation rates of ~3 m per 1000 years. Rapid sedimentation results from high influxes of terrigenous materials. The main source of clastic sediments has been the Colorado River.

[12] The dominant mode of faulting in the Gulf of California is controlled by right-lateral strike-slip transform faults connecting short pull-apart basins. The sequence of transform faults and spreading centers along the Gulf of California can be continued to the north, as far as the Salton Sea, connecting to the San Andreas fault system [e.g., *Sykes*, 1968; *Lomnitz et al.*, 1970]. The Gulf of California is an active rift between the Pacific and North American plates.

[13] Late Mesozoic and early Cenozoic subduction of the Farallon plate eastward beneath North America continued into Miocene time. The transition from a convergent to a transform plate boundary occurred with the northward and southward migration of two triple junctions [*Atwater and Molnar*, 1973]. At ~12 Ma, the oceanic spreading of the Guadalupe and Magdalena plates (southern remnant pieces of the old Farallon plate) west of Baja California ceased [*Lonsdale*, 1991], and both microplates were captured by the Pacific plate. Relative motion between the Pacific plate and North America was then partitioned into dextral strike-slip motion west of Baja California, along the Tosco-Abreojos fault zone [*Spencer and Normark*, 1979; *Normark et al.*, 1987], and east-northeast directed extension within the future Gulf of California, the so-called Proto-Gulf [*Stock and Hodges*, 1989]. From this time, Baja California moved nearly 400 km relative to North America, with 150–160 km of that motion occurring prior to 5–6 Ma [*Lonsdale*, 1991]. *Gans* [1997] proposed an alternative model in which Baja California began moving with nearly the full Pacific plate rate shortly after the end of the subduction, implying a displacement of at least 500 km.

[14] In the southern Gulf of California, seafloor spreading began in the Alarcón basin at 3.6 Ma (anomaly 2A), and in the *Stock and Hodges* [1989] and *Lonsdale* [1991] models, the plate boundary is thought to be transferred from the Pacific to the gulf not long before this time. Spreading rates from 3.6 Ma to the present have only changed at 0.78 Ma, from ~45–47 mm yr^{-1} prior to this time to 49–50 mm yr^{-1} to present [*DeMets*, 1995], where some residual Pacific-North America motion could have been accommodated by faults to the west of the Baja California peninsula [*DeMets*, 1995]. Some relative motion can still be taking place [*Spencer and Normark*, 1979; *Normark et al.*, 1987].

[15] In the northern Gulf of California, *Gastil et al.* [1973], *Gastil and Krummenacher* [1977], and *Gastil et al.* [1991] correlated distinctive deposits near San Felipe, in Baja California, and in Sonora and Tiburón Island. These tie points were confirmed by the recent work of *Oskin et al.* [2001] and *Oskin and Stock* [2003], correlating younger (Miocene) volcanic strata. This match implies a displacement of about 255 km from 6.3 Ma to the present and maybe a few tens of kilometers of additional dextral displacement prior to that time. The model of *Gans* [1997] requires an additional 200 km of right-lateral displacement to the east of the tie points, across Sonora. *Lonsdale* [1989] proposed that the original plate boundary, between circa 6 and 3 Ma, was located to the east of Angel de la Guarda island, along the Tiburón transform fault and the upper and upper Tiburón basins. Some time after 3 Ma, the old plate boundary migrated westward and was replaced by the present one, along the Salsipuedes-Ballenas channel, as the northwest extension of the Guaymas transform fault, and through the upper and upper Delfín basins [*Lonsdale*, 1989; *Stock*, 2000; *Nagy and Stock*, 2000]. The crustal structure in the northern Gulf

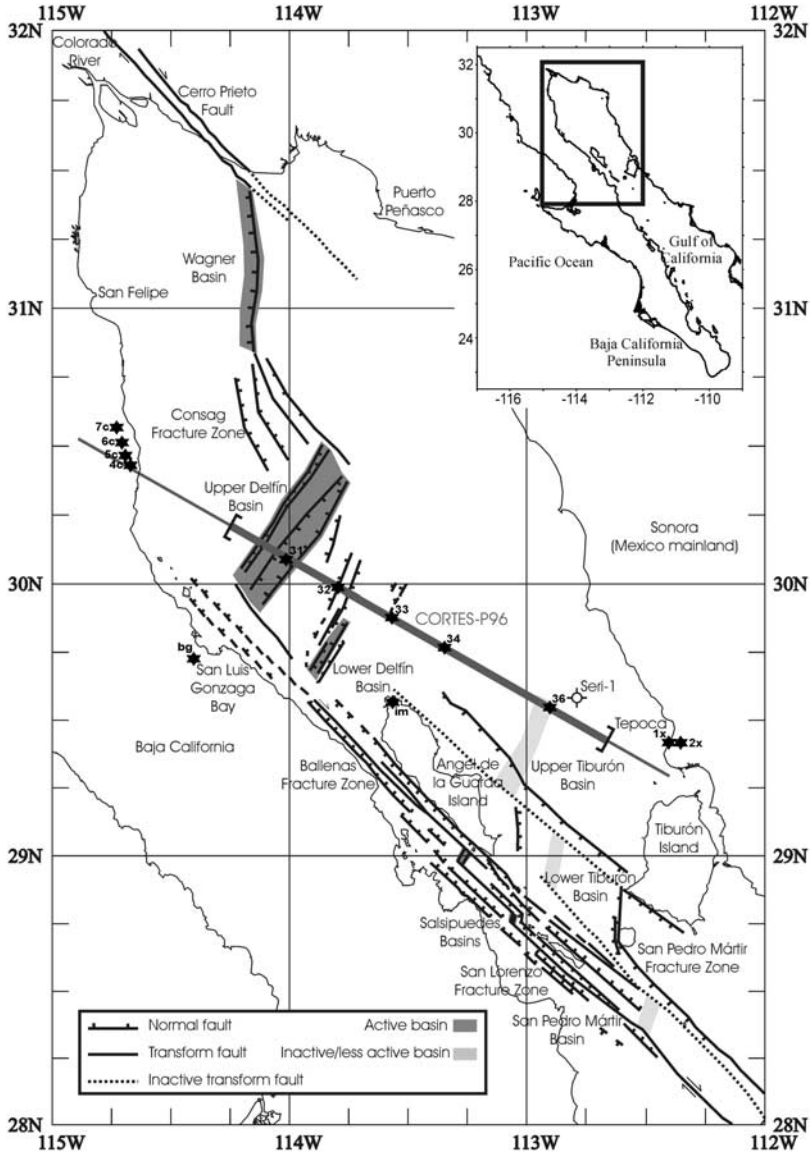

Figure 2. Tectonic map. Insert shows the location of the study area, in the northern Gulf of California. The map includes the most significant tectonic features, the main faults, and extensional basins [after *Henyey and Bischoff*, 1973; *Fenby and Gastil*, 1991] as well as the location of the wide-angle seismic line (thin gray line), the air gun shooting line/MCS line (thick gray line), and the wide-angle recording instruments (stars).

of California may show this extension migration to the west.

3. Data Sets

[16] The multidisciplinary experiment CORTES-P96 [*Dañobeitia et al.*, 1997] obtained seismic, bathymetric, and gravity data along the western margin of Mexico. The northernmost geophysical profile P313 was carried out to obtain information on the deep crustal structure of the upper Delfín basin, between San Felipe, Baja California, and Cape Tepoca, Sonora (Figure 2). In this 280-km-long NW-SE profile, deep multichannel near-vertical reflection seismics (MCS), densely sampled (80 m) refraction/wide-angle reflection seismics and gravity data were recorded. This data set was simultaneously acquired using a 50 L (3000 cubic inches) marine air gun source array provided by the R/V *Hespérides*, shooting along a 180-km-long line. This energy was recorded as MCS by a 2.4-km-long 96-channel streamer and as wide-angle by five ocean bottom seismometers (OBS) offshore, and eight portable seismic instruments onshore. Six land stations were located at the ends of the shooting line and 2 stations were located off line. Four of the online land stations were located in the Baja California Peninsula, near San Felipe, and 2 of them were on the Mexican mainland, to the north of Tiburón Island, near Cape Tepoca. One of the off-line recording instruments was installed in San Luis Gonzaga bay and the other in Mejía Island, at the northern tip of Angel de la Guarda Island and near the center of the shooting line. One OBS was situated

Table 1. Processing Sequence and Parameters for the MCS Data

Process	Parameters
Format change	SEG-D to SEG-Y
Antialias	filtering 60 Hz
Resampling	to 8 ms
Trace editing	Bad traces killed
Butterworth band-pass filtering	6–10–55–60 Hz
Geometry specification	CDP gathering
Spherical divergence/correction	velocity model
Trace equalization	RMS trace equalization
Predictive deconvolution	maximum lag 300 ms, minimum lag 16 ms
Velocity analysis	TWTT < 4 s
Wide-angle to RMS velocity conversion	TWTT > 3 s
NMO correction	velocity model
Stack	velocity model
Gazdag migration	velocity model
Time-variant band-pass filter	0–4 s, 6–10–50–55 Hz; 6–12 s, 6–10–15–20 Hz
Noise reduction	f–k
GAGC	1000 ms window

near the axis of the upper Delfín basin, one was in the center of the upper Tiburón basin and three more were deployed in the area between the basins.

[17] Gravity data were recorded aboard the R/V *Hespérides* using a BGM-3 gravimeter, calibrated in Acapulco (Mexico) just prior to the beginning of the experiment, using two land gravimeters (Lacoste-Romberg and Worden). Navigation, potential and echo sounder data were recorded at 5 s intervals. Eötvös correction was applied using a Gaussian filtered navigation. Spikes were removed manually. Finally, gravity was decimated to a 30 s interval. For the present work, gravity data were further decimated to 1 data point each 2.5 km.

[18] This data set allowed us to obtain a detailed image of the crust and determining a detailed model of the distribution of the *P* wave velocities and densities with depth.

4. Methods of Interpretation

[19] The processing sequence and the parameters applied to the MCS data are summarized in Table 1. Because of the difficulty of obtaining clear enough velocity spectra for the deeper part of the section, the wide-angle velocities were converted to RMS velocities to be used to process the line for TWTT greater than 3–4 s. Conversely, the structural information provided by the MCS section has been used to improve the wide-angle and gravity model. Attenuation of multiple energy was achieved mainly by frequency filtering and predictive deconvolution.

[20] Minimal processing was applied to the wide-angle data. Each receiver gather was band-pass filtered (3–12 Hz Butterworth), and after that, normalized amplitude was used for representation purposes. Events were correlated on each gather, and the arrival time of each event was picked for input into the modeling procedure. The main arrivals comprise sedimentary refractions (first arrivals for the shorter source-recorder distances) as well as Moho reflections. Rarely, reflections from beneath the sedimentary section are observed. Wide-angle seismic data were interpreted through ray-tracing forward modeling, using the code of *Zelt and Smith* [1992]. The 2-D velocity-depth model includes travel time and amplitude calculations and was used

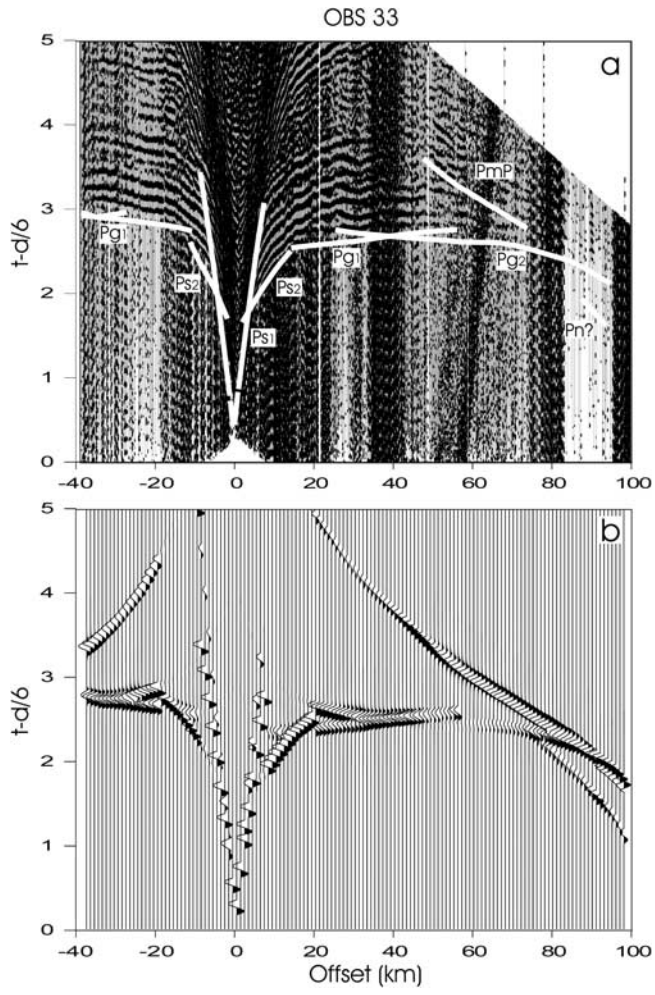

Figure 3. Wide-angle record section for OBS 33. Example of OBS wide-angle record section with (a) calculated travel times and (b) synthetic seismograms. See its location in Figure 1. Ps1 and Ps2 correspond to the sedimentary refracted waves, Pg1 and Pg2 are basement refracted arrivals, *Pn* is the refracted phase in the upper mantle, and *PmP* are the reflected waves in the Moho.

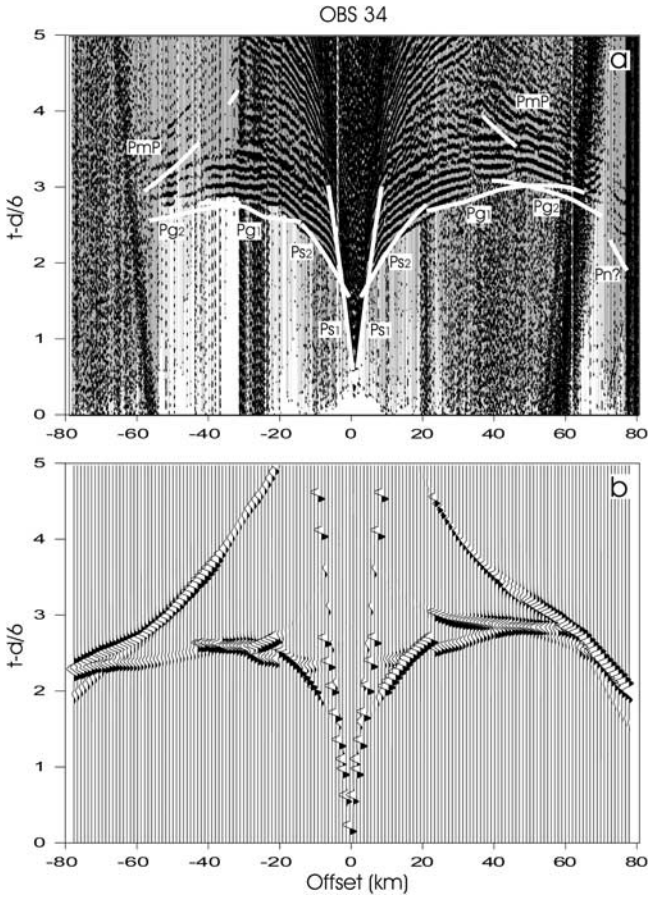

Figure 4. Wide-angle record section for OBS 34. Example of OBS wide-angle record section with (a) calculated travel times and (b) synthetic seismograms. See its location in Figure 1.

to produce synthetic seismograms. Intermediate models were modified until travel time and amplitude agreement with the data was achieved. The relative amplitudes of the phases used in the interpretation were compared with the observed ones and adjusted by forward modeling where necessary. Because the data were recorded by all the receivers simultaneously, there is reversed ray coverage in the model, in the area covered by the air gun shots.

[21] To improve the wide-angle seismic modeling of the uppermost crust (namely, the sedimentary cover), we used selected velocity analyses from the MCS line, in areas without either tectonic disturbances or side echo seismic events. The results were averaged to obtain the mean values used in the starting model for wide-angle seismics. The OBS data set provided more detail of the velocity distribution in the upper kilometers of the transect.

[22] The modeling results are discussed below, together with the main features of the seismic sections. Representative observed wide-angle data are shown together with the calculated synthetic seismograms (Figures 3–7). Wide-angle data have been plotted as receiver gathers. The lines drawn in the wide-angle record sections indicate the calculated travel time curves of the different seismic phases. For clarity, the ray-tracing model (Figure 8) is displayed with a much reduced number of rays. Signal-to-noise ratio was improved by weight-summing five adjacent traces. The wide-angle record sections are plotted with a reduction velocity of 6.0 km s^{-1} and with amplitudes normalized to the maximum of each trace. The vertical component for both OBS and land stations has been used.

[23] With few exceptions, the wide-angle seismic model presented here reproduces the observed travel times with an error less than 0.1 s. Certain amplitude and arrival time fluctuations could not be modeled, either due to local heterogeneities or due to limitations in the modeling methodology such as diffractions that can not be generated with the *Zelt and Smith* [1992] method. In the worst case, the misfit is 0.3 s. An example of such diffracted waves can be seen in Figure 5. On the basis of perturbations applied to the velocities and depths of the model, producing variations in travel times greater than 0.1 s, we estimate that the mean errors for the velocities are about ±0.1 km s^{-1}. Using the same criteria, the mean uncertainties for the depth values are between ±0.5 km or better for the upper crust to approximately ±1 km for the lower crust. These errors can vary from place to place depending on ray density and multiplicity of coverage by different recording stations.

[24] The 2-D gravity modeling has been carried out with an algorithm [*Talwani et al.*, 1959] that calculates the

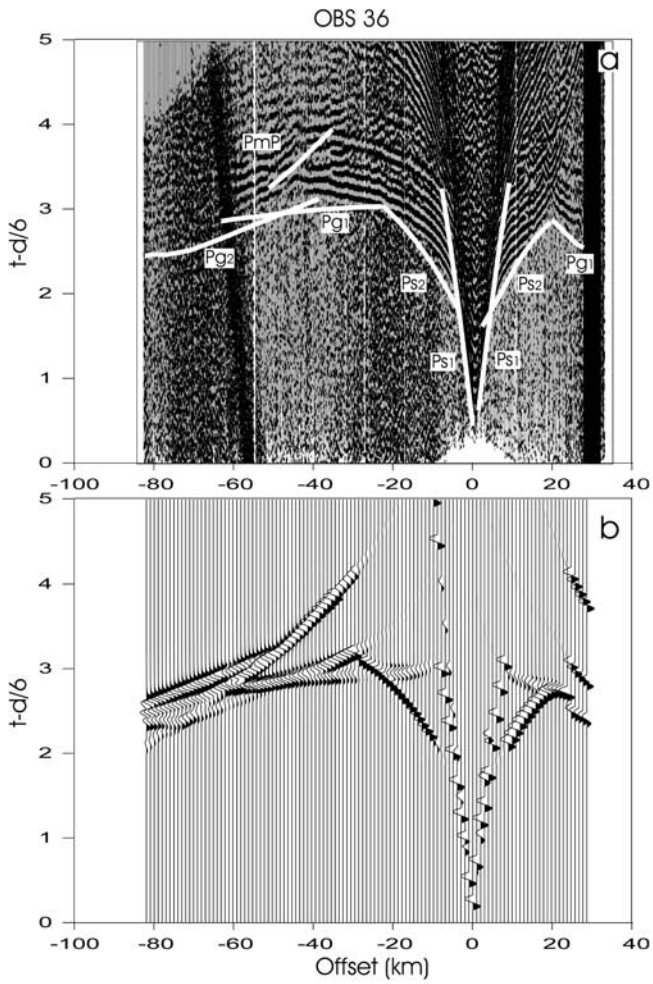

Figure 5. Wide-angle record section for OBS 36. Example of OBS wide-angle record section with (a) calculated travel times and (b) synthetic seismograms. Note the diffractions at positive offsets. See its location in Figure 1.

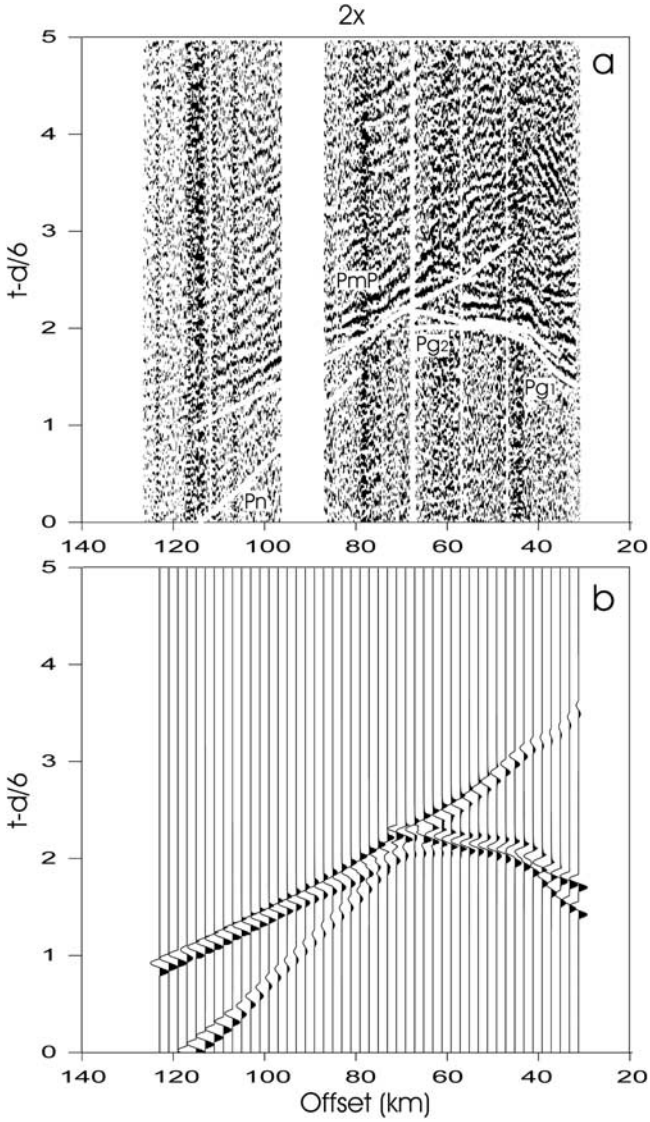

Figure 6. Wide-angle record section for land instrument 2x. Example of wide-angle land record section located on Mexico mainland, with (a) calculated travel times and (b) synthetic seismograms. See its location in Figure 1.

gravimetric contribution of 2-D polyhedra. This modeling is based on the velocity-depth interpretations deduced from seismic data. The density-depth model was obtained by converting the *P* wave velocity model using the empirical velocity-density relationship proposed by *Ludwig et al.* [1970]. Calculated densities have been rounded up to ± 50 kg m^{-3}. The geometry of both, the wide-angle velocity-depth and the density-depth models, matches exactly, excepting an area of the upper mantle discussed later.

5. Wide-Angle and Gravity Data Interpretation

[25] In the first 10 km offset in all OBS wide-angle record sections (Figures 3, 4 and 5), beyond the direct water wave, arrival times show strong curvature, having apparent velocities that range from 1.7 to 2.3 km s^{-1}, common velocities for marine sedimentary rocks. Arrivals beyond this offset range define longer and straighter branches with higher apparent velocities. The only prominent second arrivals correspond to reflections from the Moho discontinuity, although some other inconspicuous reflected waves can also be detected. Refracted waves from the uppermost mantle could only be identified for some land records (Figures 6 and 7) with good enough signal-to-noise ratio, and some OBS where adequate longer offsets were acquired (Figures 3 and 4), but with a poor signal-to-noise ratio. Although the refracted phases from the upper mantle are unreversed or not completely reversed, the travel times of these arrivals (mainly the land stations) and the additional information provided by the amplitude relationship between the Moho reflected waves and the first arrivals at different stations, allow us to suggest a mean velocity value for the uppermost mantle of $\sim$7.9 km s^{-1}. More seismic data, especially from OBS longer offset recordings and higher-energy sources are needed to establish the mantle velocity distribution of this active rift area.

[26] The lack of clear wide-angle reflections other than the reflection from the Moho indicates that there are no significant velocity discontinuities, except between the lower crust and the upper mantle (Figure 8). The modeled

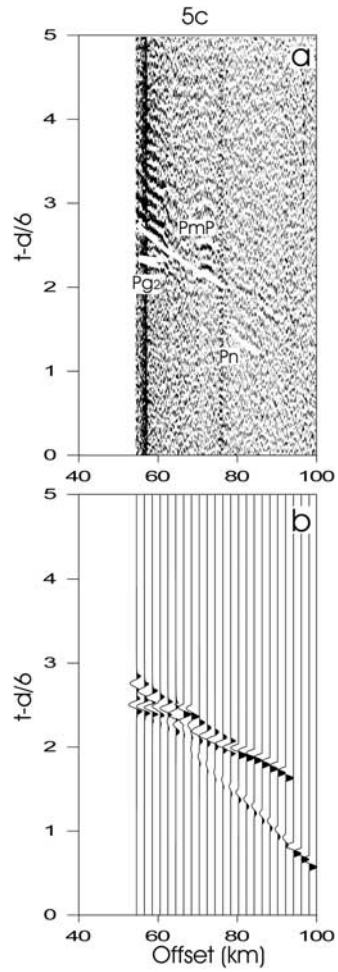

Figure 7. Wide-angle record section for land instrument 5c. Example of wide-angle land record section located in the Baja California Peninsula, with (a) calculated travel times and (b) synthetic seismograms. Note the lack of sedimentary phases. See its location in Figure 1.

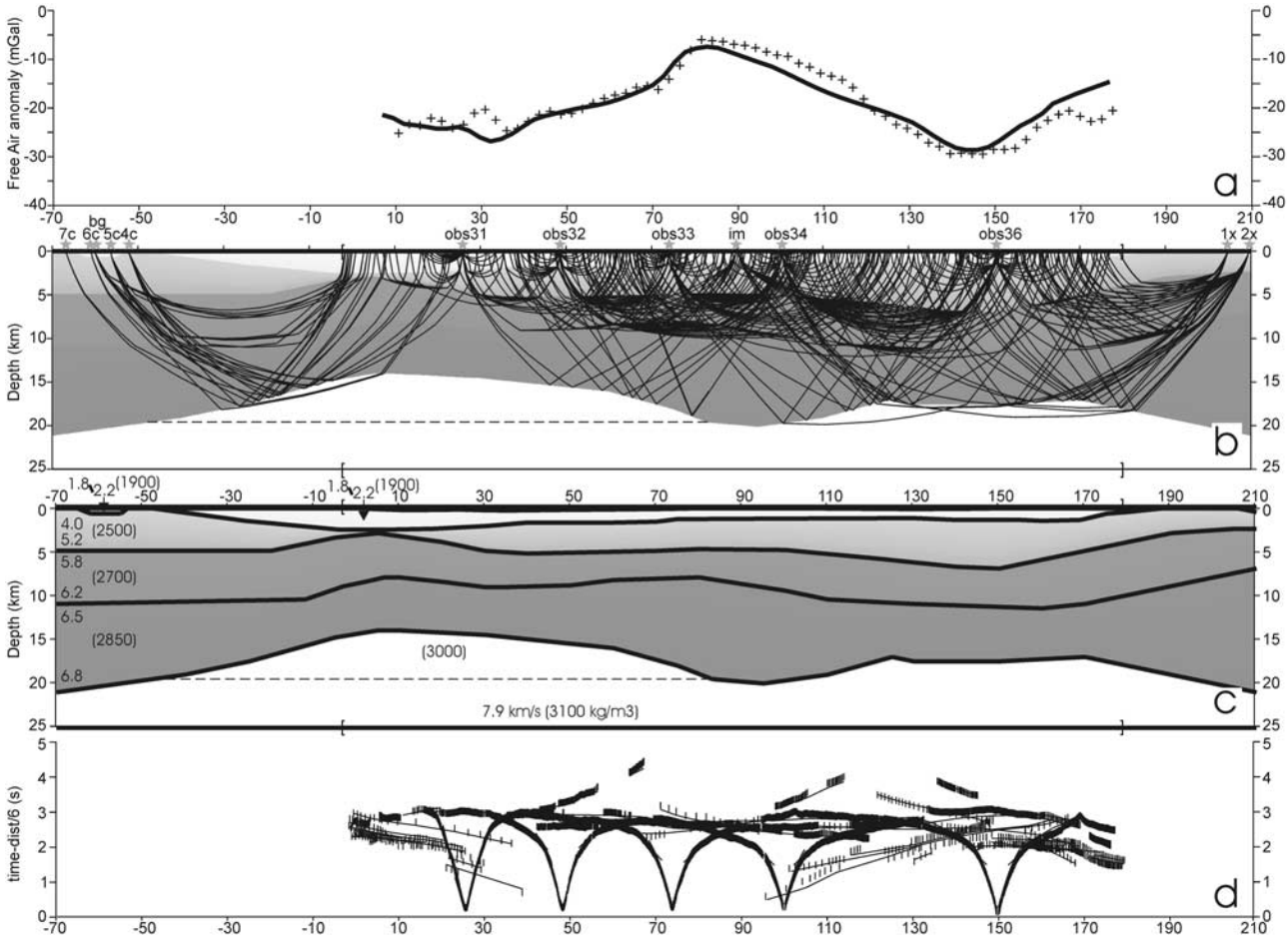

Figure 8. The 2-D velocity and density model. (a) Free-air gravity anomaly, including observed (crosses) and calculated (solid line) values. (b) Projected locations of the wide-angle recording instruments (stars) and ray coverage. For clarity, a reduced number of the actual calculated rays are represented. Brackets mark the limits of the MCS line. (c) *P* wave seismic velocity and density versus depth final model. The different layers are indicated mainly for clarity purposes because of the strong vertical velocity gradients. (d) Observed (vertical bars) and calculated (lines) travel times.

crust can be divided into three main layers. They include, from top to bottom, the sedimentary layer, a layer with velocity greater than 5.8 km s^{-1}, here referred to as the middle crust, and the lower crust, with velocity greater than 6.5 km s^{-1}.

[27] The sedimentary layer was modeled in two sections. The total thickness of this layer ranges from 3 km in the Sonora margin to more than 7 km under upper Tiburón basin. The upper sedimentary layer is characterized by a *P* wave velocity of 1.8–2.2 km s^{-1} and a mean density of 1900 kg m^{-3}. Its thickness varies from 0 to 2.6 km, with the maximum thickness located in the upper Delfín basin. The lower sedimentary layer is modeled with a conspicuous vertical velocity gradient from 4.0 km s^{-1} just below the first sedimentary layer to 5.2 km s^{-1} at the base. In this layer, the mean density is 2500 kg m^{-3}. Its maximum thickness of 6 km is reached in the upper Tiburón basin. PEMEX interpretations of commercial seismic lines only associate degrees of compaction to sedimentary levels but it was not possible to suggest accurate ages, due to the scarcity of biostratigraphic markers [*Pérez-Cruz*, 1980]. Possible ages for the sedimentary units can be supposed based on the 3 km kyr^{-1} sedimentation rate proposed by *Van Andel* [1964] and *Pérez-Cruz* [1980] and applying a correction for the effect of compaction.

[28] The middle crust also presents a vertical velocity gradient, from 5.8 to 6.2 km s^{-1}. Its mean density is 2700 kg m^{-3}. The thickness of this layer is nearly constant around 5 km. In the lower crust, the *P* wave velocity increases from 6.5 to 6.8 km s^{-1} and its mean density is 2850 kg m^{-3}. This layer almost doubles in thickness from 6 km below upper Delfín and upper Tiburón basins to 11 km in the area located between the basins. The velocity of the upper mantle is inferred to be ~7.9 km s^{-1} and its mean density is 3100 kg m^{-3}.

[29] Seismic stations located off line (San Luis Gonzaga bay and Mejía Island) were not included in the first stage of the wide-angle modeling. Once corrected for sedimentary thickness and projected into the line, the deeper arrivals were in good agreement with the current model, thus indicating a certain bidimensionality in the crustal structure.

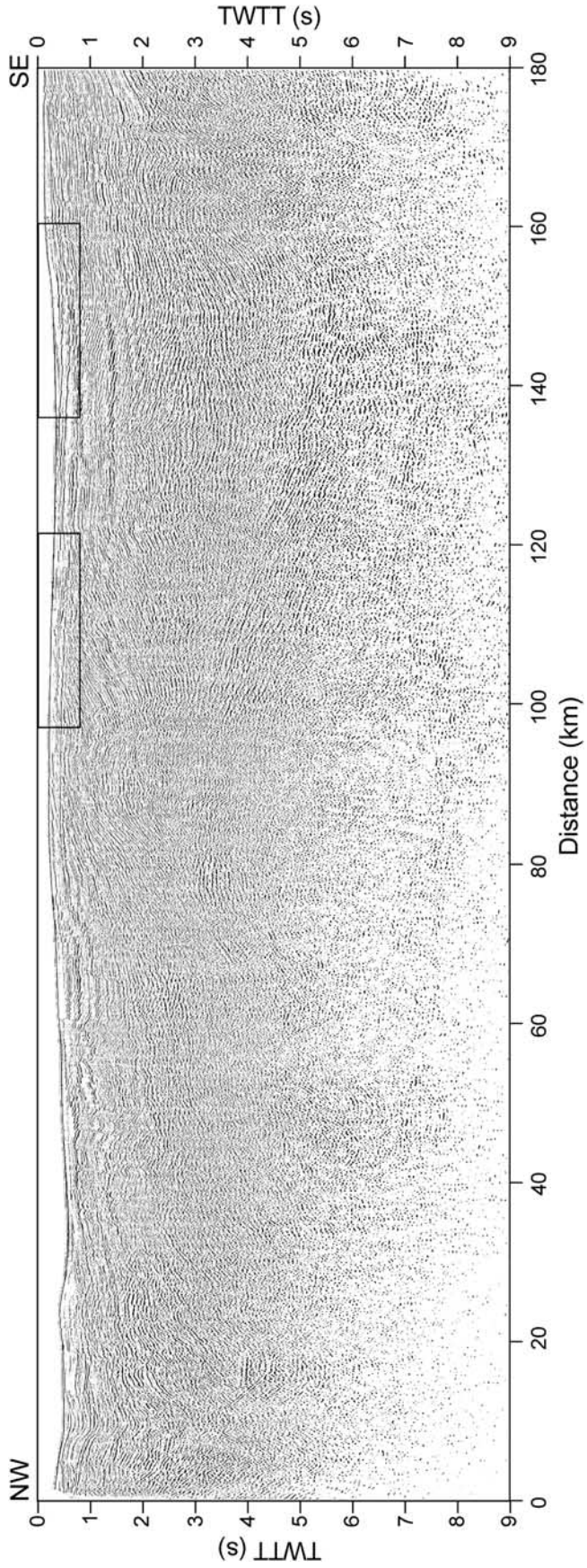

Figure 9. Time-migrated MCS time section. Note the reflectivity between 3 and 6 s TWTT at 60–160 km and the subtle Moho reflections at ~7 s. The boxes mark the location of the detailed views of Figure 10.

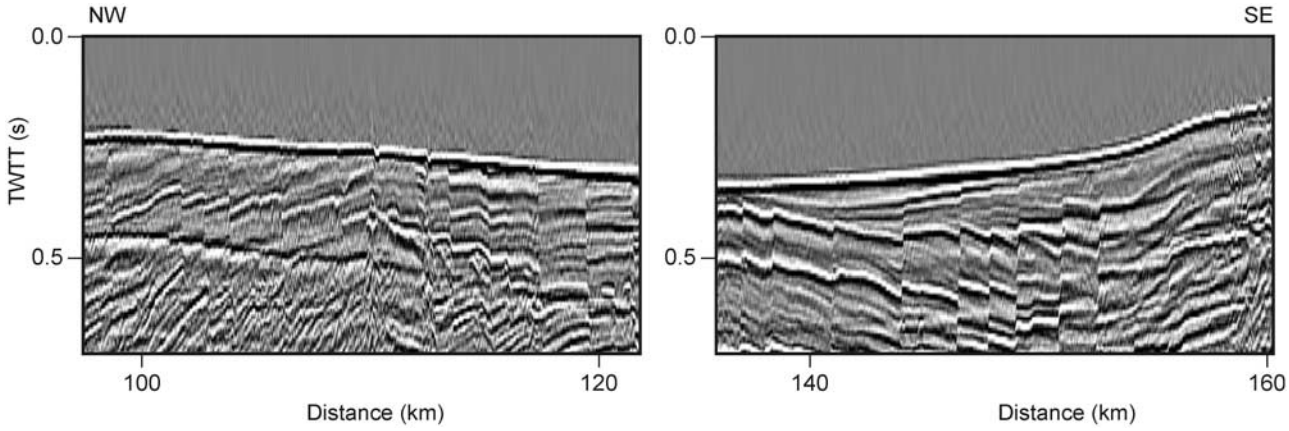

Figure 10. Detail of two areas located in the upper Tiburón basin, showing recent faulting. See its location in Figure 9.

[30] In the gravity model, the low-amplitude (20 mGal peak to peak) Free Air gravity anomalies correlate with the deep structure, especially the sedimentary and crustal thicknesses. The bathymetric influence is small, due to depth variation along the record line of less than 100 m. We found that we could not construct a gravity model with an acceptable fit to the observed data if we used the seismic Moho location and a mean mantle density. However, when we introduced a low-density body of 3000 kg m^{-3} below the upper Delfín basin, the fit between modeled and observed gravity was excellent. There is not enough seismic information to confirm the existence of an associated velocity anomaly in this area.

[31] The seismic and gravity modeling constrains two thinned crustal areas, corresponding respectively to the upper Delfín and the upper Tiburón basins. On both ends of the profile, a progressive thickening of the continental crust is observed. Our results indicate a crustal thickness of 19 km at the basin margins (below the coastline) and 14 km and 17 km below the upper Delfín and upper Tiburón basins, respectively. In the area between the basins, the crust thickens to a maximum of 19.5 km.

6. MCS Data Interpretation

[32] The MCS section (Figure 9) shows clear normal faulting in the entire line, with some of the faults reaching the surface and associated with scarps in the sea bottom (Figure 10). No faults could be traced beneath the mid-crustal set of reflectors. The apparent vergence of the faults reverses from northwestward to southeastward in three locations, corresponding to a basement uplift near the center of the seismic section (distance of 100 km) and to the surface projections of the depocenters of the basins (20 and 150 km). The sedimentary cover shows faulting that appears to change angle with depth in upper Tiburón basin and some of these faults cut the ocean bottom. This active faulting can be explained either by continued active extension in upper Tiburón basin or by subsidence due to the sedimentary load. The deeper, more consolidated sediments are characterized by reflections with low amplitudes but moderate lateral continuity, especially in their upper part. The upper unconsolidated sediments are widely distributed across both basins and are characterized by laterally continuous internal reflections. Reflectors within these upper sediments are truncated at the seabed over the basement high indicating active erosion to the north of Angel de la Guarda Island.

[33] The basement is clearly identified only to the southeast, starting a rapid shallowing at 160 km toward the Mexico mainland margin. In the southeast extreme of the seismic section, the basement reflectors dip southeast and are cut by normal faults, suggesting southeast tilting of downdropped basement blocks. Those faulted blocks are the probable counterpart of the sharp western margin of the gulf extensional province, where in much of northern Baja California the rift margin is represented by the ~100 km long, east dipping, San Pedro Mártir fault. To the northwest of 150 km, the geometry of the basement is more poorly constrained and in some sections the aid of the wide-angle interpretations is necessary.

[34] The middle and lower crust show some coherent reflections in localized areas. In the northwesternmost 20 km of the seismic section, below upper Delfín basin, a series of diffractions cannot be related to any other structure such as faulting and so it is speculated that they may mark the location of magmatic bodies. At 50 km distance, in the lower crust, there is a group of diffractions, also possibly related to magmatic intrusive bodies.

[35] We estimated the location of the crust-mantle boundary (Moho) using the wide-angle data, the gravity modeling and detectable reflectivity in the MCS section. The deepest reflections in the seismic section are events that occur between 6 and 7 s. These events fall in the depth range of the Moho defined by wide-angle reflections and by gravity interpretations. Moho-related reflectivity occurs mainly beneath upper Tiburón basin, although inconspicuous reflections can be traced under upper Delfín basin. The apparent relief on Moho reflections under the southeastern edge of the MCS section is a velocity pull-up effect due to the varying thickness of the overlying low-velocity sedimentary fill.

[36] A prominent feature of the seismic section is the presence of a southeast dipping zone of reflectivity within the middle to lower crust, which extends horizontally between 60 and 160 km, under upper Tiburón basin and

under the basement high that separates both basins. This reflectivity runs from near the top of the basement to the lower crust and merges into a zone of lower crustal reflectivity at around 5–6 s, under the depocenter of upper Tiburón basin and slightly to the southeast. This reflectivity band appears to cut half of the crust and is a well defined reflective zone ~2 km thick. The reflectivity zone has an apparent dip of ~15° between 100 and 140 km. We considered an out of plane origin for the reflectivity band, but there is no bathymetric feature in a suitable orientation to cause this reflectivity by side swipe of energy traveling through the water column. It is also unlikely that an upper crustal structure can be responsible for this reflectivity because the gravity does not show any appropriate anomaly. Also, the reflectivity is parallel to the base of the sediments of the upper Tiburón basin, supporting the interpretation that these are genuine reflection events. For these reasons we think that it is likely that the dipping reflections came from a fault zone. Further discontinuous segments of this reflector band can be traced to the northwest between 60 and 80 km, where they appear with the opposite dip.

7. Discussion and Conclusions

7.1. General Crustal Structure

[37] As pointed out before, only *Phillips* [1964], using explosives as seismic energy sources and sonobuoys as refraction recording instruments, obtained some previous deep crustal information in the study area. Although *Phillips* [1964] could not confidently determine the Moho depth in the area, he suggested a value of 24–25 km and velocities of 7.8–8.3 km s^{-1} below one station located near −31 km along the profile presented in our work. He also suggested a Moho depth of 18.4 km at 31°N–114°W, in the Consag fracture zone and Wagner basin area. The three refraction locations that can be compared with our model can be projected to −31, 60 and 156 km in our transect (sonobuoys 3, 7, and 11 of *Phillips* [1964]). *Phillips* [1964] interpreted in these locations a series of layers with constant velocities: values in the range 1.77 to 2.15 km s^{-1} for the uppermost sediments, 4.11–5.09 km s^{-1} for the lower sediments, 5.37–5.67 km s^{-1} for the middle crust, and 6.58–6.73 km s^{-1} for the lower crust. Those values are good estimates of the velocities interpreted by us. However, our results imply the presence of rather strong vertical velocity gradients as high as 0.4 km s^{-1} km^{-1} for the lower sediments and 0.08 km s^{-1} km^{-1} for the middle crust. The presence of vertical velocity gradients in the crust of the Gulf of California was initially suggested by *Henyey and Bischoff* [1973]. They even proposed that it may be more realistic to interpret a continuous velocity with depth function rather than velocities in terms of discrete layers in this area, particularly near the spreading centers. Strong vertical velocity gradients were also observed in the Imperial Valley region [e.g., *Fuis et al.*, 1984].

[38] The middle and lower crust, with *P* wave velocities from 5.8 to 6.8 km s^{-1} and conspicuous vertical velocity gradients, similar to the values reported by *Fuis et al.* [1984] for their ''metasedimentary basement'' layer (5.65–6.6 km s^{-1}), hence can be interpreted as sediments metamorphosed to lower greenschist facies, as suggested by these researchers for the Imperial Valley region. However, the seismic and gravity deep structure of the crust in the active upper Delfín and upper Tiburón basins area can not be geologically explained by the extensive intrusion of magmatic dikes, sills and/or magma chambers, because they will produce a high *P* wave velocity and high-density anomaly in the lower crust, which is not observed. Nevertheless, in the absence of any other obvious structures, the observation of a small number of isolated diffractions in this zone may be related to the presence of magmatic bodies. The low density of the upper mantle beneath the upper Delfín basin can be related to a high-temperature zone.

[39] The interpreted structure, that shows a thinning of the crust below the upper Tiburón basin, is consistent with extension in this area. Although the normal faults observed in the area reach the surface at some places, indicating that they are still active today, the faulting seems to be much less active than in the upper Delfín basin [*González-Fernández et al.*, 1999]. Most of the faulting in upper Delfín basin is active, reaching the sea bottom and even producing bathymetric scarps [*Henyey and Bischoff*, 1973; *Persaud et al.*, 2003; *González-Fernández et al.*, 1999]. The faults that affect the basement in the southeastern part of the profile are continuous up to the surface. The faulting is scattered in the entire section, indicating that the deformation is distributed over the whole area, as originally proposed by *Henyey and Bischoff* [1973], based on shallow data.

[40] As seismic velocity is principally dependent on pressure, temperature, and mineralogy [*Christensen*, 1982], wide-angle results can be used to constrain the bulk composition of the lower crust. The seismic velocities found for the lower crust, in the range 6.5–6.8 km s^{-1}, suggest a mineralogical composition of more quartz-feldspar rich felsic than mafic rocks [*Christensen*, 1982; *Furlong and Fountain*, 1986]. A 6.5–6.8 km s^{-1} lower crust is unlikely to be dominant mafic. The relatively low velocities of the lower crust indicate that there is not a process of underplating or intense intrusion of mantle material into the crust, although a low amount of mafic dikes may exist.

[41] The concave upward shape of the Moho beneath the upper Tiburón basin can be explained by the intense sedimentary infill, so the lower crust cannot isostatically support the weight. The subsidence/infill ratio was won by the infill, producing the downward flexure of the Moho observed in the southeastern half of the profile, between 110 and 165 km in the model (Figures 8 and 9).

7.2. Middle-Lower Crust Reflectivity

[42] The series of subparallel southeast dipping reflectors observable in the MCS section, from 100 to 160 km, are the most striking features of our data (Figures 9 and 11). This feature can also be recognized between 60 and 80 km as northwest dipping reflectors. A possible interpretation of these interfaces is a mylonite zone related to detachment surfaces. Alternatively, this reflectivity can be due to other causes, such a compressional structure that predates any extension (Laramide?).

[43] Seismic characteristics of mylonite zones are sufficient to produce reflections in crystalline rocks [*Fountain et al.*, 1984; *Jones and Nur*, 1984; *McDonough and Fountain*, 1988]. Reflectors related to mylonite zones present certain lateral discontinuity that can arise from a combination of structural complexity of the layering and a low signal-to-

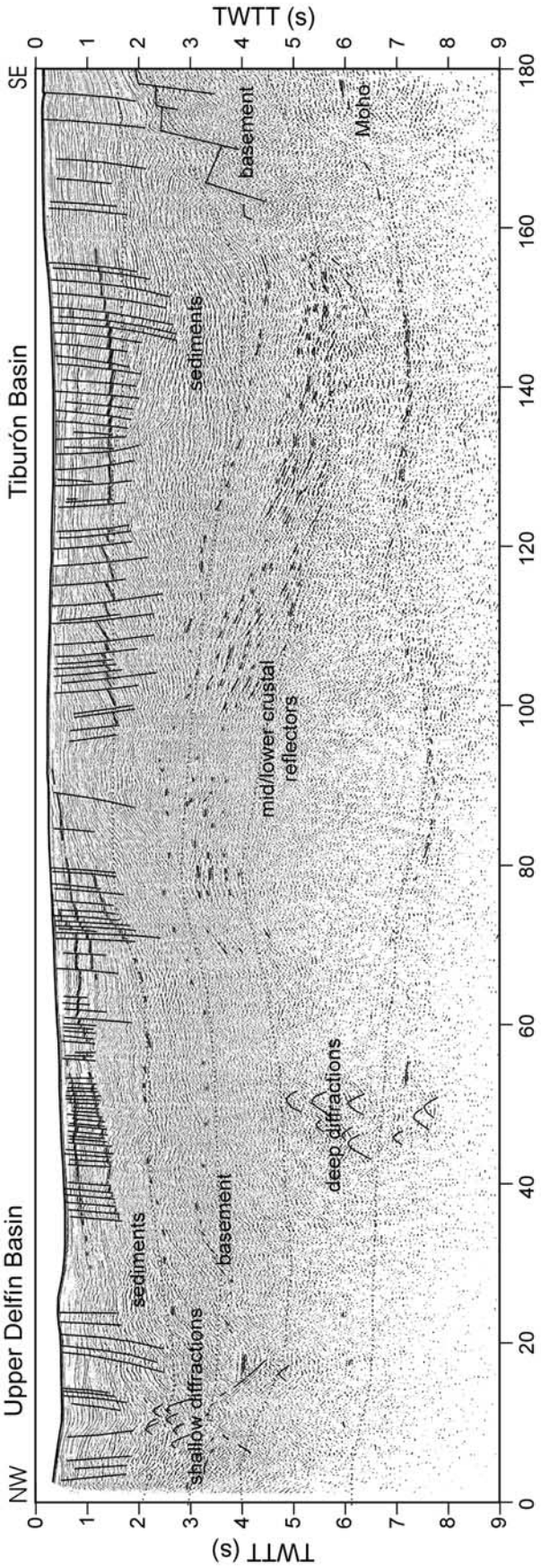

Figure 11. Sketch of the interpretation of the MCS seismic section. Diffractions can be observed in the unmigrated section. Dotted lines correspond to the layers indicated on the wide-angle model (see Figure 8).

noise ratio. Mylonite reflectors show relatively high amplitudes that vary laterally and are multicyclic in character. Synthetic seismograms for mylonite zones of laminated geometry show complex multicyclic reflections with a wave train about 0.2 s long and with amplitudes up to twice or even three times those generated by a single interface, due to constructive interference of reflected waves [*Fountain et al.*, 1984].

[44] The first direct evidence of the seismic reflectivity of mylonites was provided by a seismic reflection profile over a mylonite zone exposed in the Kettle dome metamorphic core complex, in northeastern Washington, as a complex zone of multicyclic reflections [*Hurich et al.*, 1985]. This mylonite zone provides a good example of a fault zone formed at midcrustal levels that is now exposed and directly correlatable with seismic data. The zone of reflections spans about 1 s TWTT. An example of a bigger-scale, basement-involved, upper crustal low-angle normal fault seismic image is the COCORP profile across the Sevier Desert detachment in the eastern Basin and Range province of western Utah [*Allmendinger et al.*, 1983]. This profile shows a series of strong, rather continuous, multicyclic reflections that extend over horizontal distances of 70 km and that can be traced from near the surface down to over 5 s two-way travel time (12–15 km depth), with an average dip of 12°. However, the zone of reflections corresponding to the Sevier Desert Detachment fault is much more restricted in TWTT (usually spanning only 0.1–0.3 s TWTT), whereas the zone identified in the present study is apparently 1.0 s TWTT or more, in thickness on the interpretive cross section (Figure 11). The zone of reflectors corresponding to the Sevier Desert Detachment is also much more continuous than the zone seen in the present data. It is also important to notice that *Anders and Christie-Blick* [1994] suggest that the dipping reflectivity in the COCORP seismic profile does not correspond to a shear zone. Furthermore, caution should be taken that there can be some ambiguity in the true dip of the reflectors due to the lack of three-dimensional control.

[45] Line 7 in Bothnian and Baltic Echoes from the Lithosphere (BABEL) showed dipping reflections at 12 to 25 km depth [*Law and Snyder*, 1997]. Updip projection suggests that these reflections may have originated from acoustic impedance contrasts within a crustal-scale brittle-ductile shear zone, the Shingö shear zone, which crops out along the Swedish coast. Here, the reflective zone has a thickness near 4 s TWTT and is discontinuous. Amplitude and phase coherency of seismic reflections from shear zones vary considerably, depending on focusing and defocusing effects, thin layer tuning and variations in velocity [*Law and Snyder*, 1997]. Other areas where thick (~1 s TWTT or more) dipping reflectors in the middle or lower crust have been observed and related to mylonite zones are offshore British Islands [e.g., *Reston*, 1990], the Eagle Pass below the Pinaleño Mountains core complex in southeast Arizona [*Kruger and Johnson*, 1994], or the Buckskin-Rawhide core complex in southwestern Arizona [*Hauser et al.*, 1987], among others.

7.3. Metamorphic Core Complex

[46] The possible interpretation of the mid crustal reflectivity as a mylonite zone and its spatial association with the relatively thick lower crust under the center of the seismic section, allow us to explain this reflectivity as a detachment shear zone over a metamorphic core complex.

[47] Metamorphic core complexes are areas in which ductily deformed medium to high-grade metamorphic rocks, originated in the middle or lower crust, have been unroofed and are exposed at or near the surface [*Coney*, 1980]. Some low-angle detachment faults, common to all metamorphic core complexes, have large translational displacements, in excess of several tens of kilometers. The rate of translation along master faults can be very rapid (>1 cm yr^{-1}) [*Davis and Lister*, 1988]. Uplift of the footwall is rapid, while sedimentation continues in the hanging wall.

[48] Most metamorphic core complexes are asymmetric when viewed perpendicular to the direction of tectonic transport. On one side of the complex, the lower plate mylonitic fabrics and overlying detachment fault both dip gently in the direction of upper plate transport, and there is less than 10° to 20° of discordance between this main mylonitic zone and the detachment fault. On the opposite side, the mylonitic zone diverges downward from the detachment fault and rolls over to a moderate to gentle dip opposed to the direction of upper plate transport. The discordance between this back-dipping mylonitic zone and the detachment may be of 30° or more [*Reynolds and Lister*, 1990]. The top of the back-dipping mylonitic zone is sometimes referred to as the mylonite front [*Davis and Lister*, 1988]. The main mylonitic zone can be traced into the back-dipping zone with little change in character and little or no decrease in the intensity of the fabric. The back-dipping mylonitic zone can be explained as a down-folded continuation of the main shear zone [*Reynolds and Lister*, 1990]. An alternate explanation for the back-dipping mylonitic zone is a layer of relatively strong midcrustal rock, rotated and flexed above the ductile crust beneath it [*Wernicke*, 1992].

7.4. Lower Crust Flow

[49] One evidence that the lower crust has flowed is that the crustal thickness variations are smoothed out relative to the strong thickness variations of the lower crust. There are not many differences in elevation/bathymetry either, although this can also be explained by the strong sedimentary infill. In the neighboring Basin and Range province there is evidence that lower crustal flow occurred, almost synchronously with regional extension [e.g., *Gans*, 1987; *Block and Royden*, 1990; *Kruse et al.*, 1991; *Bird*, 1991]. In the absence of such flow, large variations in Moho topography would have been produced. Moreover, the creep rate of the upper mantle is generally less than that of the lower crust when they are at the same temperature [*McKenzie et al.*, 2000].

[50] With adequate crustal thickness and heating from igneous intrusions or addition of water, the lower crust will be able to flow [e.g., *Kruse et al.*, 1991; *McKenzie and Jackson*, 2002]. The lower crustal flow will only occur where the crustal thickness exceeds a certain value, depending on the local conditions [*McKenzie et al.*, 2000; *McKenzie and Jackson*, 2002]. Thus, although the crustal thinning will be developed slowly in extensional tectonics in the presence of the equalizing effect of the lateral flow, this flow is not always successful in removing crustal

thickness contrasts, so it will eventually stop, due to necking and cooling [*Block and Royden*, 1990].

[51] Water is likely to be added to the lithosphere, above the now extinct Farallon subduction zone. These can raise the homologous temperature, making flow more likely [*McKenzie and Jackson*, 2002]. In addition to necking and cooling, dehydration can play an important role stopping the crustal thinning.

[52] Underplating can produce effects similar to lower crustal flow, reducing crustal thickness variations. However, the relatively low seismic velocities found in our section are more suggestive of a lower crustal flow mechanism. *Furlong and Fountain* [1986] propose seismic velocities ranging from 6.8 to 8.0 km s^{-1} for a layer of underplated materials. On the other hand, if mantle-derived melt is emplaced within the lower crust, the resulting velocity signature will depend on the composition of the original lower crust and can be difficult to detect. The presence of diffractions in the MCS section located in the lower crust suggests the existence of at least localized sill-like bodies. These diffractions are situated near the low-density anomaly of the upper mantle interpreted from gravity data, which might be related to an area of partial melting.

7.5. Mode of Extension

[53] We propose that the mode of extension in the study area has changed from core complex mode to narrow rift mode, in the sense of *Buck* [1991]. Buck proposed that the continental lithosphere can extend in three distinct ways, depending on whether or not the locus of extension remained fixed and on the efficiency of lower crustal flow. For a range of thermal gradients, the thermal softening of the lower crust allows it to creep at a low level of applied stress (ductile behavior, simple shear deformation), while the upper crust and the uppermost part remain stronger [*Brace and Kohlstedt*, 1980]. The three modes defined by *Buck* [1991] are core complex mode (concentrated upper crustal extension with lower crustal thinning), wide rift mode (uniform crustal and mantle lithospheric thinning over a width greater than the lithospheric thickness) and narrow rift mode (concentrated crustal extension and mantle rise). Models by *Buck* [1991] and *Hopper and Buck* [1996] imply a temporal progression from one model to the other. They proposed that the southern Basin and Range may be an example of a region which has passed through all three modes of extension. The first period involved core complex formation in Arizona. It was followed by wide rift Basin and Range extension with distributed upper crustal extension. The last phase includes the Salton Sea and Rio Grande narrow rifts.

[54] The interpreted crustal structure in the northern Gulf of California shows strong thickness variations in the lower crust, thus evidencing lower crustal flow. However, we can not rule out the possibility of an overthickened lower crust prior to the gulf extension. Additionally, taking into account the moderate heat flow (values of $\sim$100–120 mW m^{-2} [*Henyey and Bischoff*, 1973; *Sánchez-Zamora et al.*, 1991]), in this conditions the core complex is predicted by the model of *Buck* [1991]. Crustal thickness variations produce lateral pressure gradients within the crust, driving flow of the weak lower crust. The flow of the lower crust spreads out the local crustal thinning variations required for either low strain or collapse mechanisms needed to produce a wide rift, and inhibit localized upwelling of asthenosphere to shallow levels for a narrow rift [*Wernicke*, 1992]. Midcrustal rocks are exhumed in isostatic response to the removal of the hanging wall and the inflow of the lower crust. The identification of a crustal root beneath the center of the interpreted seismic line suggests that isostasy has been a driving force in the unroofing of the footwall. There are a number of metamorphic core complexes identified in Sonora, Mexico, thus suggesting the plausibility of this mode of extension in the area. Numerous exposures of detachments and their metamorphic substrate form a nearly continuous belt from Sonora, Mexico, to southern British Columbia, Canada, referred to as the Cordilleran metamorphic core complexes [*Crittenden et al.*, 1980; *Coney*, 1980; *Armstrong*, 1982; *Henry and Aranda-Gómez*, 1992]. Crustal-scale extension was widespread in Sonora at $\sim$12 Ma [*Henry and Aranda-Gómez*, 1992]. Extensions of 100–200 km during brief intervals of only 2–3 Myr occurred during the Miocene and late Oligocene in different areas of the southwestern United States [e.g., *Anderson et al.*, 1972; *Wernicke et al.*, 1982; *Glazner and Bartley*, 1984].

[55] Following *Hopper and Buck* [1996], during the core complex phase, there is locally high strain over a narrow area while the crustal thinning is spread over a wide area. Lower crustal flow is directed into the rift zone, reducing the Moho topography. Analog models by *Gartrell* [1997] show that the ductile lower crust acts as an isostatic equalizer, thinning under the thicker areas of the upper crust and, to the contrary, thickening under the thinner areas of the brittle upper crust. The regions of extension are situated, usually moderately offset, above the region of upwelling ductile lower crust. Because of the distributed crustal thinning, the cooling of the lower crust raises the effective viscosity and decreases the efficiency of the lower crustal flow. Moreover, after enough stretching, the lower crust almost thins out, so it cannot flow fast enough. In due time, the extension thus evolves to a wide rift. This phase involves both upper Tiburón and upper Delfín basins having simultaneous extension. An area that has been thermally weakened during the core complex phase is left behind. There is now a preexisting weakness in the crust that locates the future narrow rift [see *Hopper and Buck*, 1996, Figure 7]. Active faulting located in the entire seismic section, although with noticeably higher activity in the upper Delfín basin, indicates that the present mode of extension may be transition between wide and narrow rift, perhaps more evolved toward the narrow rift mode. The mode change is a gradual transition rather than a sharp boundary. Extreme necking and continental breakup will occur in the future.

7.6. Evolution With Time

[56] Assuming the regional tectonic model of *Stock* [2000] and *Nagy and Stock* [2000], we propose that the crustal extension was achieved initially by major low-angle detachment fault zone and the formation of large tilted fault blocks that began at 6–4 Ma. As proposed by *Mutter et al.* [1989], the detachment surface may have nucleated near the sediment-basement contact, which acted as a stress guide. The upper Tiburón basin area lacks evidence for magmatism. The main phase of crustal thinning in upper

Tiburón basin and the proposed metamorphic core complex development ended about 3–2 Ma. We estimated a maximum displacement of ~100 km based on the total extent of the midcrustal reflectors. That implies that the detachment operated at a maximum average slip rate of ~40 km Myr^{-1}. We interpret this first phase of extension to have thinned upper Tiburón basin crust from ~30 km, similar to the value observed for the Basin and Range [*Allmendinger et al.*, 1983], to less than the present value of 19 km. Since the time when the extension migrated from upper Tiburón to upper Delfín basin, around 3–2 Ma, the crust can be thickened by up to 3 km of sediments, if we suppose a sedimentation rate of 3 km kyr^{-1} [*Van Andel*, 1964; *Pérez-Cruz*, 1980]. Compaction can reduce this estimate significantly. The basement may have been almost exhumed (isostatically uplifted) in the center part of the section, at 4–3 Ma, from midcrustal level to subsurface depth, therefore an uplift rate of 4 or 5 mm yr^{-1} can be calculated.

[57] The only pre-6 Ma upper crust in the seismic section is represented by the tilted blocks in the southwestern part of the line. Other similar blocks are exposed nearby, in Tiburón Island. In agreement with *Oskin et al.* [2001] and *Oskin and Stock* [2003], the rest of the original upper crust is entirely missing. The proposed lower crustal flow has prevented the development of oceanic crust in this area.

[58] In a second phase, at around 2 Ma, the locus of extension migrated from upper Tiburón to upper Delfín basin and the mode of extension shifted, changing progressively from core complex to narrow rift, to an area characterized by high-angle normal faults and some magmatism, with no evidence of crustal detachment faulting. Activity on the earlier detachment system has probably ceased except for the effects of subsidence due to the sedimentary overburden.

[59] Gravity interpretation provides evidence of a low-density area of the upper mantle below the upper Delfín basin. However, available seismic data are insufficient to detect any velocity anomaly. The density anomaly may indicate the presence of melt. Diffractions located to the southeast in the bottom of this basin, probably related to sills, seem to confirm this interpretation. Another shallower reflector can be also interpreted as a magma reservoir. If these interpretations are correct, and assuming that strain within the upper mantle parallels the crust-mantle interface, enhanced melt production, due to adiabatic decompression, is taking place beneath upper Delfín basin, the present locus of maximum extension in the northern Gulf of California.

[60] **Acknowledgments.** This work could not have been possible without the aid of the captains and crews of R/Vs *Hespérides*, *Altair*, and *Humboldt*. Special thanks to Hubert Fabriol (CICESE-BRGM), Remy Louat (ORSTOM-IRD) and Tony Monfret (ORSTOM-IRD). Also, we thank many technicians and students that participated in the different activities inland. Acquisition and processing of the gravity and seismic data were funded by CICYT Spanish project ANT-182/94-C01/02; the Secretaría de Marina de México; CICESE projects 644107 and 644114; CONACYT projects 0894PT, 28317T, and 28318T; and Convenio CONACYT/CSIC and INSU-France. The first author also thanks funding by Dirección General de Investigación Científica y Enseñanza Superior EX96-02876832, Ministerio de Educación y Cultura (Spain). Finally, we would like to thank the anonymous reviewers for their constructive comments.

References

Allmendinger, R. W., J. W. Sharp, D. Von Tish, L. Serpa, L. Brown, S. Kaufman, and J. Oliver (1983), Cenozoic and Mesozoic structure of the eastern Basin and Range province, Utah, from COCORP seismic-reflection data, *Geology*, *11*, 532–536.

Anders, M. H., and N. Christie-Blick (1994), Is the Sevier Desert reflection of west-central Utah a normal fault?, *Geology*, *22*, 771–774.

Anderson, R. E., R. L. Longwell, R. L. Armstrong, and R. F. Marvin (1972), Significance of K-Ar ages of Tertiary rocks from the Lake Mead region, Nevada-Arizona, *Geol. Soc. Am. Bull.*, *83*, 273–288.

Armstrong, R. L. (1982), Cordilleran metamorphic core complex from Arizona to southern California, *Annu. Rev. Earth. Planet. Sci.*, *10*, 129–154.

Atwater, T. M., and P. Molnar (1973), Relative motion of the pacific and North American plates deduced from sea-floor spreading in the Atlantic, Indian and South Pacific oceans, in *Proceedings of the Conference on Tectonic Problems of the San Andreas Fault System*, edited by R. Kovach and A. Nur, *Stanford Univ. Publ. Geol. Sci.*, *16*, 136–148.

Bird, P. (1991), Lateral extrusion of lower crust from under high topography, in the isostatic limit, *J. Geophys. Res.*, *96*, 10,275–10,286.

Block, L., and L. H. Royden (1990), Core complex geometries and regional scale flow in the lower crust, *Tectonics*, *9*, 557–567.

Brace, W. F., and D. L. Kohlstedt (1980), Limits on lithospheric stress imposed by laboratory experiments, *J. Geophys. Res.*, *85*, 6248–6252.

Buck, W. R. (1991), Modes of continental lithospheric extension, *J. Geophys. Res.*, *96*, 20,161–20,178.

Christensen, N. (1982), Seismic velocities, in *Handbook of Physical Properties of Rocks II*, edited by R. S. Carmichael, pp. 1–228, CRC Press, Boca Raton, Fla.

Coney, P. J. (1980), Cordilleran metamorphic core complexes: An overview, in *Cordilleran Metamorphic Core Complexes*, edited by M. D. Crittenden Jr., P. J. Coney, and G. H. Davis, *Mem. Geol. Soc. Am.*, *153*, 7–31.

Couch, R. W., G. E. Ness, O. Sánchez-Zamora, G. Calderón-Riveroll, P. Dogin, V. Plawman, S. Coperude, B. Huehn, and W. Gumma (1991), Gravity anomalies and crustal structure of the Gulf and Peninsular Province of the Californias, in *The Gulf and Peninsular Province of the Californias*, edited by J. P. Dauphin and B. R. Simoneit, *AAPG Mem.*, *47*, 25–45.

Crittenden, M. D., Jr., P. J. Coney, and G. H. Davis (Eds.) (1980), *Cordilleran Metamorphic Core Complexes*, *Mem. Geol. Soc. Am.*, *153*, 490 pp.

Curray, R. J., et al. (1982), *Initial Reports of the Deep Sea Drilling Project*, vol. 64, 1313 pp., U.S. Govt. Print. Off., Washington, D. C.

Dañobeitia, J. J., D. Córdoba, L. A. Delgado-Argote, F. Michaud, R. Bartolomé, M. Farran, R. Carbonell, F. Núñez-Cornú, and the CORTES-P96 Working Group (1997), Expedition gathers new data on crust beneath Mexican west coast, *Eos Trans. AGU*, *78*(49), 565, 572.

Davis, G. A., and G. S. Lister (1988), Detachment faulting in continental extension: Perspectives from the southwestern U.S. Cordillera, *Spec. Pap. Geol. Soc. Am.*, *218*, 133–159.

Delgado-Argote, L. A. (2000), Evolución tectónica y magmatismo Neógeno de la margen oriental de Baja California central, Ph.D. thesis, 175 pp., Univ. Nac. Auto. de Mexico, Mexico, D. F.

DeMets, C. (1995), A reappraisal of seafloor spreading lineations in the Gulf of California: Implications for the transfer of Baja California to the Pacific plate and estimates of Pacific-North America motion, *Geophys. Res. Lett.*, *22*, 3545–3548.

Einsele, G. (1982), Mechanism of sill intrusion into soft sediment and expulsion of pore water, *Initial Rep. Deep Sea Drill. Proj.*, *64*, 1169–1176.

Fabriol, H., L. A. Delgado-Argote, J. J. Dañobeitia, D. Córdoba, A. González, J. García-Abdeslem, R. Bartolomé, B. Martín-Atienza, and V. Frías-Camacho (1999), Backscattering and geophysical features of volcanic rifts offshore Santa Rosalía, Baja California Sur, Gulf of California, Mexico, *J. Volcanol. Geotherm. Res.*, *93*, 75–92.

Fenby, S. S., and R. G. Gastil (1991), Geologic-tectonic map of the Gulf of California and surrounding areas, in *The Gulf and Peninsular Province of the Californias*, edited by J. P. Dauphin and B. R. Simoneit, *AAPG Mem.*, *47*, 79–83.

Fountain, D. M., C. A. Hurich, and S. B. Smithson (1984), Seismic reflectivity of mylonite zones in the crust, *Geology*, *12*, 195–198.

Frías-Camacho, V. M., L. A. Delgado-Argote, and J. J. Dañobeitia (1999), Interpretación de rasgos estructurales y volcánicos de Canal Las Ballenas y Cuenca Delfín Inferior, Golfo de California, a partir de imágenes de reflectividad, *GEOS Unión Geofís. Mex.*, *19*, 220.

Fuis, G. S., W. D. Mooney, J. H. Healy, G. A. McMechan, and W. J. Lutter (1984), A seismic refraction survey of the Imperial Valley region, California, *J. Geophys. Res.*, *89*, 1165–1189.

Furlong, K. P., and D. M. Fountain (1986), Continental crust underplating: Thermal considerations and seismic-petrologic consequences, *J. Geophys. Res.*, *91*, 8285–8294.

Gans, P. B. (1987), An open-system, two layer crustal stretching model for the eastern Great Basin, *Tectonics*, *6*, 1–12.

Gans, P. B. (1997), Large-magnitude Oligo-Miocene extension in southern Sonora: Implications for the tectonic evolution of northwest Mexico, *Tectonics*, *16*, 388–408.

Gartrell, A. P. (1997), Evolution of rift basins and low-angle detachments in multilayer analog models, *Geology*, *25*, 615–618.

Gastil, R. G., and D. Krummenacher (1977), Reconnaissance geology of coastal Sonora between Puerto Lobos and Bahia Kino, *Geol. Soc. Am. Bull.*, *88*, 189–198.

Gastil, R. G., D. V. Lemone, and W. J. Stewart (1973), Permian fusilinids from near San Felipe, Baja California, *AAPG Bull.*, *57*, 746–747.

Gastil, R. G., et al. (1991), The relation between the Paleozoic strata on opposite sides of the Gulf of California, in *Studies of Sonoran Geology*, edited by C. Jacques-Ayala, *Spec. Pap. Geol. Soc. Am.*, *254*, 7–17.

Glazner, A. F., and J. M. Bartley (1984), Timing and tectonic setting of Tertiary low-angle normal faulting and associated magmatism in the southwestern United States, *Tectonics*, *3*, 385–396.

González-Fernández, A., J. J. Dañobeitia, D. Córdoba, L. A. Delgado-Argote, R. Carbonell, and R. Bartolomé (1999), Estructura de la litosfera en el Alto Golfo de California a partir de datos de sísmica de reflexión, gran ángulo y gravimetría, *GEOS Unión Geofís. Mex.*, *19*, 219.

Hauser, E. C., J. Gephart, T. Latham, J. Oliver, S. Kaufman, L. Brown, and I. Lucchitta (1987), COCORP Arizona transect: Strong crustal reflections and offset Moho beneath the transition zone, *Geology*, *15*, 1103–1106.

Henry, C. D., and J. J. Aranda-Gómez (1992), The real southern Basin and Range: Mid- to late Cenozoic extension in Mexico, *Geology*, *20*, 701–704.

Henyey, T. L., and J. L. Bischoff (1973), Tectonic elements of the northern part of the Gulf of California, *Geol. Soc. Am. Bull.*, *84*, 315–330.

Hopper, J. R., and W. R. Buck (1996), The effect of lower crustal flow on continental extension and passive margin formation, *J. Geophys. Res.*, *101*, 20,175–20,194.

Hurich, C. A., S. B. Smithson, D. M. Fountain, and M. C. Humphreys (1985), Seismic evidence of mylonite reflectivity and deep structure in the Kettle dome metamorphic core complex, Washington, *Geology*, *13*, 577–580.

Irving, E. (1970), The Mid-Atlantic Ridge at 45°N: Oxidation and magnetic properties of basalt: Review and discussion, *Can. J. Earth Sci.*, *7*, 1528–1538.

Jones, T., and A. Nur (1984), The nature of seismic reflections from deep crustal fault zones, *J. Geophys. Res.*, *89*, 3153–3171.

Klitgord, K. D., J. D. Mudie, J. L. Bischoff, and T. L. Henyey (1974), Magnetic anomalies in the northern and central Gulf of California, *Geol. Soc. Am. Bull.*, *85*, 815–820.

Kruger, J. M., and R. A. Johnson (1994), Raft model of crustal extension: Evidence from seismic reflection data in southeast Arizona, *Geology*, *22*, 351–354.

Kruse, S., M. McNutt, J. Phipps-Morgan, L. Royden, and B. Wernicke (1991), Lithospheric extension near Lake Mead, Nevada: A model for ductile flow in the lower crust, *J. Geophys. Res.*, *96*, 4435–4456.

Larson, P. A., J. D. Mudie, and R. L. Larson (1972), Magnetic anomalies end fracture-zone trends in the Gulf of California, *Geol. Soc. Am. Bull.*, *83*, 3361–3368.

Law, A., and D. B. Snyder (1997), Reflections from a mylonitized zone in central Sweden, *J. Geophys. Res.*, *102*, 8411–8425.

Lomnitz, C., F. Mooser, C. R. Allen, J. N. Brune, and W. Thatcher (1970), Seismicity and tectonics of the northern Gulf of California region, Mexico—Preliminary results, *An. Inst. Geofís. Int.*, *10*, 37–48.

Lonsdale, P. (1985), A transform continental margin rich in hydrocarbons, Gulf of California, *AAPG Bull.*, *69*, 1160–1180.

Lonsdale, P. (1989), Geology and tectonic history of the Gulf of California, in *The Geology of North America*, vol. N, *The Eastern Pacific Ocean and Hawaii*, edited by E. L. Winterer, D. M. Hussong, and R. W. Decker, pp. 499–521, Geol. Soc. of Am., Boulder, Colo.

Lonsdale, P. (1991), Structural patterns of the Pacific floor offshore of Peninsular California, in *The Gulf and Peninsular Province of the Californias*, edited by J. P. Dauphin and B. R. Simoneit, *AAPG Mem.*, *47*, 87–125.

Ludwig, W. F., J. E. Nafe, and C. L. Drake (1970), Seismic refraction, in *The Sea*, vol. 4, *New Concepts of Sea Floor Evolution*, edited by A. E. Maxwell, pp. 53–84, Wiley-Interscience, Hoboken, N. J.

McDonough, D. T., and D. M. Fountain (1988), Reflection characteristics of a mylonite zone based on compressional wave velocities of rock samples, *Geophys. J. R. Astron. Soc.*, *93*, 547–558.

McKenzie, D., and J. Jackson (2002), Conditions for flow in the continental crust, *Tectonics*, *21*(6), 1055, doi:10.1029/2002TC001394.

McKenzie, D., F. Nimmo, J. A. Jackson, P. B. Gans, and E. L. Miller (2000), Characteristics and consequences of flow in the lower crust, *J. Geophys. Res.*, *105*, 11,029–11,046.

Mutter, J. C., R. L. Larson, and Northwest Australia Study Group (1989), Extension of the Exmouth Plateau, offshore northwestern Australia: Deep seismic reflection/refraction evidence for simple and pure shear mechanisms, *Geology*, *17*, 15–18.

Nagy, E. A., and J. M. Stock (2000), Structural controls on the continent-ocean transition in the northern Gulf of California, *J. Geophys. Res.*, *105*, 16,251–16,269.

Ness, G. E., and M. Lyle (1991), A seismo-tectonic map of the Gulf and peninsular Province of the Californias, in *The Gulf and Peninsular Province of the Californias*, edited by J. P. Dauphin and B. R. Simoneit, *AAPG Mem.*, *47*, 71–78.

Normark, W. R., J. Spencer, and J. Ingle (1987), Geology and Neogene history of the Pacific continental margin of Baja California, in *Geology and Resource Potential of the Continental Margin of Western North America and Adjacent Ocean Basins*, *Earth Sci. Ser.*, vol. 6, edited by D. Scholl, A. Grantz, and J. Vedder, pp. 449–472, Circum-Pac. Counc. for Energy and Miner. Resour., Houston, Tex.

Oskin, M., and J. Stock (2003), Pacific-North America plate motion and opening of the Upper Delfín basin, northern Gulf of California, Mexico, *Geol. Soc. Am. Bull.*, *115*, 1173–1190.

Oskin, M., J. Stock, and A. Martín-Barajas (2001), Rapid localization of Pacific-North America plate motion in the Gulf of California, *Geology*, *29*, 459–462.

Paz-López, S. (2000), Procesamiento e interpretación de datos sísmicos y gravimétricos en el norte del Golfo de California, Master thesis, 134 pp., Cent. de Invest. Cient. y Educ. Super. de Ensenada, B. C., Mexico.

Paz-López, S., A. González-Fernández, J. J. Dañobeitia, L. A. Delgado-Argote, and D. Córdoba (2000), Estructura sísmica y gravimétrica de la corteza en el centro norte del Golfo de California, *GEOS Unión Geofís. Mex.*, *20*, 317.

Pérez-Cruz, G. A. (1980), Exploración petrolera de la porción noroccidental del Golfo de California, *Bol. Asoc. Mex. Geofís. Explor.*, *21*, 3–4, 80–128.

Persaud, P., J. M. Stock, M. S. Steckler, A. Martín-Barajas, J. B. Diebold, A. González-Fernández, and G. S. Mountain (2003), Active deformation and shallow structure of the Wagner, Consag, and Delfín Basins, northern Gulf of California, Mexico, *J. Geophys. Res.*, *108*(B7), 2355, doi:10.1029/2002JB001937.

Phillips, R. P. (1964), Seismic refraction studies in the Gulf of California, in *Marine Geology of the Gulf of California*, edited by T. H. Van Andel and G. G. Shor, *AAPG Mem.*, *3*, 90–121.

Reston, T. J. (1990), The structure of the crust and the uppermost mantle offshore Britain: Deep seismic reflection profiling and crustal cross-sections, in *Exposed cross-sections of the continental crust*, *NATO ASI Ser., Ser. C*, vol. 317, edited by M. H. Salisbury and D. M. Fountain, 603–621, Kluwer Acad., Norwell, Mass.

Reynolds, S. J., and G. S. Lister (1990), Folding of mylonitic zones in Cordilleran metamorphic core complexes: Evidence from near the mylonitic front, *Geology*, *18*, 216–219.

Sánchez-Zamora, O., P. Doguin, R. W. Couch, and G. E. Ness (1991), Magnetic anomalies of the northern Gulf of California: Structural and thermal interpretations, in *The Gulf and Peninsular Province of the Californias*, edited by J. P. Dauphin and B. R. Simoneit, *AAPG Mem.*, *47*, 377–401.

Saunders, A. D., D. J. Fornari, and M. A. Morrison (1982), The composition and emplacement of basaltic magmas produced during the development of continental margins: The Gulf of California, Mexico, *J. Geol. Soc. London*, *139*, 335–346.

Smith, W. H. F., and D. T. Sandwell (1997), Global seafloor topography from satellite altimetry and ship depth soundings, *Science*, *277*, 1957–1962.

Spencer, J. E., and W. R. Normark (1979), Tosco-Abreojos fault zone: A Neogene transform plate boundary within the Pacific margin of Baja California, Mexico, *Geology*, *7*, 554–557.

Stock, J. M. (2000), Relation of the Puertecitos Volcanic Province, Baja California, Mexico, to development of the plate boundary in the Gulf of California, in *Cenozoic Tectonics and Volcanism of Mexico*, edited by H. Delgado-Granados, G. Aguirre-Díaz, and J. M. Stock, *Spec. Pap. Geol. Soc. Am.*, *334*, 143–156.

Stock, J. M., and K. V. Hodges (1989), Pre-Pliocene extension around the Gulf of California and the transfer of Baja California to the Pacific plate, *Tectonics*, *8*, 99–115.

Sykes, L. R. (1968), Seismological evidence for transform faults, sea-floor spreading and continental drift, in *The History of the Earth's Crust, A Symposium*, edited by R. A. Phinney, pp. 120–150, Princeton Univ. Press, Princeton, N. J.

Talwani, M., J. L. Worzel, and M. Landesman (1959), Rapid gravity computation for two-dimensional bodies with application to the Mendocino submarine fracture zone, *J. Geophys. Res.*, *64*, 49–59.

Van Andel, T. H. (1964), Recent marine sediments of Gulf of California, in *Marine Geology of the Gulf of California*, edited by T. H. Van Andel and G. G. Shor, *AAPG Mem.*, *3*, 216–301.

Vogt, P. R., C. N. Anderson, D. R. Bracey, and E. D. Schneider (1970), North Atlantic magnetic smooth zones, *J. Geophys. Res.*, *75*, 3955–3968.

Wernicke, B. (1992), Cenozoic extensional tectonics of the U.S. Cordillera, in *The Geology of North America* vol. G-3, *The Cordilleran Orogen: Conterminous U.S.*, edited by B. C. Burchfiel, P. W. Lipman, and M. L. Zoback, pp. 553–581, Geol. Soc. of Am., Boulder, Colo.

Wernicke, B., B. C. Spencer, B. C. Burchfield, and P. L. Guth (1982), Magnitude of crustal extension in the southern Great Basin, *Geology*, *10*, 499–502.

Zelt, C. A., and R. B. Smith (1992), Seismic traveltime inversion for 2-D crustal velocity structure, *Geophys. J. Int.*, *108*, 16–34.

R. Bartolomé and J. J. Dañobeitia, Unidad de Tecnología Marina, CSIC, Pg. Maritim de la Barceloneta 37-49, E-08003 Barcelona, Spain. (rafa@utm.csic.es; jjdanobeitia@utm.csic.es)

D. Córdoba, Departamento de Geofísica, Facultad de Ciencias Físicas, Universidad Complutense de Madrid, Av. Complutense s/n, E-28040 Madrid, Spain. (dcordoba@eucmos.sim.ucm.es)

L. A. Delgado-Argote and A. González-Fernández, CICESE-Geología, P.O. Box 434843, San Diego, CA 92143-4843, USA. (ldelgado@cicese.mx; mindundi@cicese.mx)

F. Michaud, Observatoire Océanologique de Villefranche, B.P. 48, F-06230 Villefranche sur Mer, France. (micho@ccrv.obs-vlfr.fr)